AFRL-RV-PS-
TR-2018-0075

CALIBRATED EARTHQUAKE LOCATIONS IN IRAN BASED ON JOINT ANALYSES OF INSAR AND SEISMIC DATA

Meng Wei, et al.

University of Rhode Island
215 South Ferry Road
Narragansett, RI 02882

16 April 2018

Final Report

AIR FORCE RESEARCH LABORATORY
Space Vehicles Directorate
3550 Aberdeen Ave SE
AIR FORCE MATERIEL COMMAND
KIRTLAND AIR FORCE BASE, NM 87117-5776

DTIC COPY

NOTICE AND SIGNATURE PAGE

AFRL-RV-PS-TR-2018-0075 HAS BEEN REVIEWED AND IS APPROVED FOR PUBLICATION IN ACCORDANCE WITH ASSIGNED DISTRIBUTION STATEMENT.

//SIGNED//	//SIGNED//
Dr. Frederick Schult	Dr. Thomas R. Caudill, Chief
Program Manager, AFRL/RVBYE	AFRL Battlespace Environment Division

REPORT DOCUMENTATION PAGE

Form Approved
OMB No. 0704-0188

1. REPORT DATE *(DD-MM-YYYY)*	**2. REPORT TYPE**	**3. DATES COVERED** *(From - To)*
16-04-2018	Final Report	10 May 2016 – 29 Dec 2017

4. TITLE AND SUBTITLE
Calibrated Earthquake Locations in Iran Based on Joint Analyses of InSAR and Seismic Data

5a. CONTRACT NUMBER
FA9453-16-C-0044

5b. GRANT NUMBER

5c. PROGRAM ELEMENT NUMBER
62601F

6. AUTHOR(S)
Meng Wei, Yang Shen, Samuel Bell, Pengcheng Shi, Melanie Wallace, Xueyang Bao, Wanpeng Feng, and Sergey Samsonov

5d. PROJECT NUMBER
1010

5e. TASK NUMBER
PPM00026926

5f. WORK UNIT NUMBER
EF129459

7. PERFORMING ORGANIZATION NAME(S) AND ADDRESS(ES)
University of Rhode Island
215 South Ferry Road
Narragansett, RI 02882

8. PERFORMING ORGANIZATION REPORT NUMBER

9. SPONSORING / MONITORING AGENCY NAME(S) AND ADDRESS(ES)
Air Force Research Laboratory
Space Vehicles Directorate
3550 Aberdeen Avenue SE
Kirtland AFB, NM 87117-5776

10. SPONSOR/MONITOR'S ACRONYM(S)
AFRL/RVBYE

11. SPONSOR/MONITOR'S REPORT NUMBER(S)
AFRL-RV-PS-TR-2018-0075

12. DISTRIBUTION / AVAILABILITY STATEMENT
Approved for public release; distribution is unlimited. (AFMC-2018-0404 dtd 19 Sep 2018)

13. SUPPLEMENTARY NOTES

14. ABSTRACT
In this one-year project (extended for another six months) to combine geodetic and seismic data to ground truth earthquakes, we made progress in the following aspects: (1) InSAR data processing and analysis. We used InSAR data from Sentinal-1A/B and Radarsat-2 to search for earthquakes in Iran after January 2011. We were able to identify 13 InSAR events from January 2011 to January 2018. Out of the 13 events, five were reported by other researchers, three were new and analyzed by us in this project, and five occurred near the end of the project (therefore only data were processed but no slip model was determined). Before 2011, 19 InSAR events have been reported. Together, the total number of InSAR-constrained events in Iran reaches 32. (2) Seismic inversion for source parameters. We used global seismic data for full waveform seismic inversion of source parameters for several earthquakes. We found that the focal mechanism is more sensitive to depth than location. Using geodetic determined depth would help provide better focal mechanism solutions. (3) Relative relocation of small earthquakes. We used surface waves to relocate small earthquakes around InSAR-determined reference earthquakes. We used several criteria including distance, magnitude difference, and depth difference to determine the pairs. Then we run cross-correlation for all the pairs. We showed that this method worked well and allowed relocation of over 250 M≥4.5 earthquakes in the USGS catalog.

15. SUBJECT TERMS
InSar, earthquake location, ground truth earthquake locations

16. SECURITY CLASSIFICATION OF:			**17. LIMITATION OF ABSTRACT**	**18. NUMBER OF PAGES**	**19a. NAME OF RESPONSIBLE PERSON**
a. REPORT	**b. ABSTRACT**	**c. THIS PAGE**			Dr. Frederick Schult
Unclassified	Unclassified	Unclassified	Unlimited	26	**19b. TELEPHONE NUMBER** *(include area code)*

This page is intentionally left blank.

Table of Contents

List of Figures and Tables

Figures

Tables

1. SUMMARY

In this one-year project (extended for another six months) to combine geodetic and seismic data to ground truth earthquakes, we made progress in the following aspects:

(1) **InSAR data processing and analysis**. We used InSAR data from Sentinal-1A/B and Radarsat-2 to search for earthquakes in Iran after January 2011. We were able to identify 13 InSAR events between January 2011 to January 2018. Out of the 13 events, five were reported by other researchers, three were analyzed by us in this project, and five occurred near the end of the project (therefore only data were processed but no slip model was determined). We developed a grid search method to determine the best fitting source model for the geodetic observation and applied it to three events. We also tested a method to reduce atmosphere noise using topography data. Before 2011, 19 InSAR events have been reported. Together, the total number of InSAR-constrained events in Iran reaches 32.

(2) **Seismic inversion for source parameters**. We used global seismic data for full waveform seismic inversion of source parameters for several earthquakes. We found that the focal mechanism is more sensitive to depth than location. Using geodetic determined depth would help provide better focal mechanism solutions.

(3) **Relative relocation of small earthquakes**. We used surface wave to relocate small earthquakes around InSAR-determined reference earthquakes. We used several criteria including distance, magnitude difference, and depth difference to determine the pairs. Then we run cross-correlation for all the pairs. We showed that this method worked well and allowed relocation of over 80 $M \geqslant 4.5$ earthquakes in the USGS catalog.

Work in this project depended on the High-Performance Computer (HPC) cluster purchased by professor Yang Shen using previous AFRL fund. The project supported a postdoctoral researcher and provided training for several students.

2. INTRODUCTION

Ground-truth (GT) events are critical in seismic monitoring and discrimination, as they provide reference for obtaining well-constrained locations, testing existing velocity/attenuation models, and discriminating earthquakes, mining activities, and chemical/nuclear explosions. Well-located events are also essential for building 3D velocity models. Most GT events in the current IASPEI catalog [Bondar and McLaughlin, 2009] are determined from seismic data and limited by the station coverage. In places with sparse seismic stations (e.g., the Mid East and Northeast Asia), GT events are few and far between, limiting our ability to monitor and discriminate seismic events in those regions. Furthermore, the current GT source information is usually limited to the location, origin time and magnitude. For waveform-based investigation, a complete GT source must include not only the location and origin time, but also the moment tensor. While the existing Centroid Moment Tensor (CMT) catalogs [Ekstrom et al., 2012] provide moment tensor solutions for large earthquakes, the earthquakes are usually not well located. The location errors, particularly in depth, affect the moment tensor solutions. So there is a large disconnect between the existing GT and CMT sources.

Interferometric synthetic aperture radar (InSAR) has been proven to be a useful tool for ground truth and locating earthquakes and nuclear tests [Vincent et al., 2003; Lohman and Simons, 2005; Barnhart et al., 2013]. For example, InSAR has provided 20 ground-truth earthquakes in southern Iran. Lohman and Simons [2005] detected four events above magnitude 4.5 between 1992-2002. Barnhart et al. [2013] detected 16 events with magnitudes above 4.8 between 2003-2011. For the InSAR ground-truth events, the center and length of the fault is usually well constrained within 0.5 km [Lohman and Simons, 2005; Barnhart et al., 2013]. However, the depth is more uncertain and the origin time is unconstrained.

We carried out a pilot study to develop a new joint geodetic and seismic method to determine the complete GT source parameters and the associated uncertainties. This pilot study focused on earthquakes in Iran. We extended the InSAR detection beyond 2011 to 2017, the end of this project. We detected additional events with InSAR observations, expanding the list of ground-truth earthquakes to a total of over 30. We inverted the source parameters using both geodetic and seismic methods. We compared their solutions, then used all the ground-truth events as the reference points and relocated earthquakes around them. Over 200 earthquakes were relocated and have location uncertainty less than 5 km. Having these GT1-5 events substantially improve our ability to locate/discriminate future seismic events in the region.

3. METHODS, ASSUMPTIONS, AND PROCEDURES

Several aspects of the research in this project have been documented in detail and are available publicly or published in professional, peer-reviewed journals. For brevity this report focuses on recent and unpublished results and provides only a brief summary of those results that are already published.

3.1. Geodetic observation and modeling

For the InSAR data, we mainly used Sentinel-1A/B from the European Space Agency and the Radarsat-2 from the Canadian Space Agency. The Sentinel data is freely available and covers April 2014 to present. The Radarsat-2 data were used for time period between 2011-2014 through collaboration with Canadian colleagues and co-authors, Dr. Sergey Samsonov and Dr. Wanpeng Feng. We focused on events after January 2011. We started with the USGS catalog and prioritized our search for shallow $M \geq 5$ events (depth < 10 km). Then we downloaded and processed InSAR data if available. For large events, the signal is obvious. For small events, multiple InSAR images were processed to confirm that the signal is not atmospheric noise.

For three selected events, we inverted surface displacement data from InSAR for fault parameters using a full grid search, rather than a computation-minimizing algorithm. Our inversion technique—a grid search—involves repeated forward modeling of the displacement from test values of model parameters. To forward model the displacement, we used the Fortran code developed by Okada [1985]. Okada [1985] uses analytical

expressions to calculate the surface deformation at a point from a rectangular slip patch in a uniform half-space. This simplified model assumes a uniform slip distribution and a pure double-couple source. One advantage of this approach is to be consistent with seismic inversion, which only use a single double-couple source and grid search for the best solution.

The Okada [1985] code requires seven parameters to describe the fault patch: length, width, latitude, longitude, depth, strike, dip, and the two components of the slip vector within the fault plane. The slip vector can also be expressed as a slip (magnitude) and rake (direction). We reduced the parameter space to eight by introducing an a priori seismic moment of the event (calculated from the seismic inversion). Once seismic moment is determined, slip is also determined based on relationship between seismic moment, fault width, and fault length.

The efficiency of the grid search algorithm is of the order n^m, where n is the number of values of each parameter, and m is the number of parameters. Because we have eight model parameters, the efficiency of the algorithm is of the order n^8, and the algorithm becomes rapidly less efficient the more values are tested for each parameter. To reduce n, we perform the grid search in two steps. In the first step, we use a coarser grid of parameter values, and in the second step, we use a finer spacing of parameter values centered around the result of the coarse grid search.

To further reduce computation time, we cut out a rectangular focus region within the interferogram and down-sample it, aiming for ~2,000-5,000 points. For the RADARSAT-2 data, we applied a mask based on the average correlation coefficient of down-sampled points in the interferogram, excluding points with correlation coefficients below 0.05.

The uncertainty of the parameters was determined based on how misfit to data changes with different parameters. The confidence level was determined by the noise level in the particular interferogram.

We also tested a method to reduce atmospheric noise using topography data. Atmospheric noise is the largest source of error in InSAR, which can be reduced by topography correction [Bekaert, 2015]. Assuming the atmosphere noise is linearly related to the topography, the interferometric tropospheric phase can be estimated from the relationship between the interferometric phase and the topography:

$$\Delta\phi_{tropo} = Kh + \Delta\phi_0$$

where K is a scale factor, h is the topography, and $\Delta\phi_0$ is a constant.

3.2. Seismic inversion

We estimated the moment tensor, the origin time, and the depth by using a strain Green tensor (SGT) method based on full-wave simulation in 3D velocity models [Zhao et al.,

2006]. Based on the theorem of reciprocity, the SGT database for the volume surrounding a reference source location can be numerically constructed by assuming an impulse source located at the receiver in each of the three orientations. Given the source *p* and station *j*, the displacement component n received at the station can be denoted by

$$b_{nm}^{j}(t,p) = \sum_{i,k=1}^{3}\left[G_{in,k}(p,t;j)M_{m}^{ik}\right] * S(t,p) \qquad (1)$$

where $b_{nm}^{j}(t,p)$ is the *n*th component of displacement at station *j* from the elementary moment tensor $\boldsymbol{M}_{\mathrm{m}}$ at source location *p*, $G_{in,k}(p,t;j)$ the Green tensor component *ik* at source location *p* due to a unit impulse force acting at station *j* in the direction *n*, and $S(t,p)$the source time function. The general moment tensor *M* is decomposed by six independent elementary moment tensors [Kikuchi and Kanamori, 1991]

$$\boldsymbol{M} = \sum_{m=1}^{N_b} \alpha_m \boldsymbol{M}_m, \qquad (2)$$

where N_b is the number of the elementary moment tensors to be inverted (up to 6). The six components of $\boldsymbol{M}$ are

$$\mathrm{M}_1 = \begin{bmatrix} 0 & 1 & 0 \\ 1 & 0 & 0 \\ 0 & 0 & 0 \end{bmatrix};\ \mathrm{M}_1 = \begin{bmatrix} 1 & 0 & 0 \\ 0 & -1 & 0 \\ 0 & 0 & 0 \end{bmatrix};\ \mathrm{M}_1 = \begin{bmatrix} 0 & 0 & 0 \\ 0 & 0 & 1 \\ 0 & 1 & 0 \end{bmatrix};$$

$$\mathrm{M}_1 = \begin{bmatrix} 0 & 0 & 1 \\ 0 & 0 & 0 \\ 1 & 0 & 0 \end{bmatrix};\ \mathrm{M}_1 = \begin{bmatrix} -1 & 0 & 0 \\ 0 & 0 & 0 \\ 0 & 0 & 1 \end{bmatrix};\ \mathrm{M}_1 = \begin{bmatrix} 1 & 0 & 0 \\ 0 & 1 & 0 \\ 0 & 0 & 1 \end{bmatrix}.$$

The normal equation for moment tensor inversion can be described as a linearized least-square problem

$$\sum_{m=1}^{N_b}\left\{\sum_{i=1}^{N} w_i \int_{t_1}^{t_2}[b_{ik}b_{im}]dt\right\}\alpha_m = \sum_{i=1}^{N} w_i \int_{t_1}^{t_2}[b_{ik}d_i]dt\,, \quad for\ k = 1,\cdots,N_b, \qquad (3)$$

where the tensor *b* can be computed from the SGTs for the station. *N* is the number of time segments, w_i a weighting factor representing waveform quality, and d_i the *i*th observed seismogram. Thus the coefficients α can be solved in a linear least-square problem at a given source location.

A grid search approach is applied to solving the inverse problem of (3) at each grid in this volume. An iterative processing is carried out through updating the moment tensor solution at each grid to minimum the misfit between the synthetics generated from (1) and observed seismograms.

This SGT-based method is more effective for the regions with significant 3D velocity variations, such as southern Iran, comparing with other source inversion methods mostly utilizing 1D earth models, such as the “Cut-And-Paste” method [Zhu and Helmberger, 1996]. The methods based on the spectral-element method numerically determine the

derivatives of the source parameters by differentiating synthetics according to the source parameters [Liu et al., 2004], which may not be efficient when the reference location is far from the true location. The SGT-based method is also more time-saving than SPECFEM-based method when the number of sources is more than that of stations, where the total number of forward waveform simulation is three times the number of stations, according to the three orientations of the impulse when Green's functions are computed. Finally, the most important advantage of the SGT-based method is the inversion part of the computation is speedy since the SGTs are pre-calculated. This indicates a better fit for real-time source inversion because the SGTs can be computed for a seismic zone before an earthquake happens.

A main hypothesis of this project is that InSAR records provide independent and nearly ground-truth constraint on the horizontal location of earthquake sources. We assume the horizontal location of a source is well-constrained from InSAR inversion, and thus use the SGT-based method to determine the moment tensor, the source depth, and the origin time. Then we compare the geodetic determined depth and seismic results.

3.3. Relative relocation using surface waves

Waveform cross-correlation has been used as an important tool for earthquake source studies, such as the characteristics of earthquake clusters and accurate source location [Poupinet et al., 1984; Shearer, 1997; Schaff and Waldhauser, 2005]. Cluster analysis by Engdahl and Bergman [2001] show GT5 for a large cluster can be achieved if a subset are well-located events with absolute locations. The double-difference algorithm [Waldhauser and Ellsworth, 2000] is used to iteratively invert relative source locations, which is especially effective for the regions with a dense distribution of seismicity. It is natural to relate the waveform cross-correlation and the double-difference method: A combination of these two methods will take advantage of the difference in location and the similarity in waveform for nearby sources [Hauksson and Shearer, 2005].

For small earthquakes with body waves that have relatively low signal-to-noise ratio, the use of surface waves for event locating is most effective and appealing [Cleveland and Ammon, 2013], particularly for regions lack of dense network such as southern Iran. The method has been used to locate earthquakes in the oceanic transform faults [McGuire, 2008; Cleveland and Ammon, 2013]. The procedure is straightforward. The waveforms from stations around the world for two chosen events are downloaded and bandpass filtered to obtain surface waves with the best signal-to-noise ratio. Surface waves with 25-50s [McGuire, 2008] or 30-80s [Cleveland and Ammon, 2013] periods are found to be suitable for these applications. The cross-correlation of surface-wave waveforms between pair events at the same station would generate the time delay. Then a simple geometrical calculation would yield the estimate of relative distance between the centroid of the two events. If one event is well located, then the other one's location can be calibrated. We used InSAR ground-truth events as references and relocated earthquakes near them based on criteria of distance, depth difference, and magnitude difference.

4. RESULTS AND DISCUSSION

4.1. Geodetic observation and modeling

We processed over 100 InSAR images. At this point, InSAR data still need to be manually setup for downloading and processing. This limited the number of events that we can inspect with InSAR. We were able to identify 13 InSAR events between January 2011 to January 2018 (Figure 1, Table 1). Most of them are located in places that had no previous InSAR-constrained earthquakes, thus provide new geographic coverage. Four of the nine events have not been reported before. The region experienced a low activity period in 2015 and 2016, which contributed to the small number of InSAR identified events. There were four new events with M≥6 occurred in November and December 2017 and one M5.5 event in January 2018. We processed InSAR data of these events and saw clear signal but we did not have time to invert for slip models. Together, this added the total number of InSAR events in Iran to 32 (Table 1). There were a number of large events between 2010-2013 should have been detected by InSAR if data were acquired.

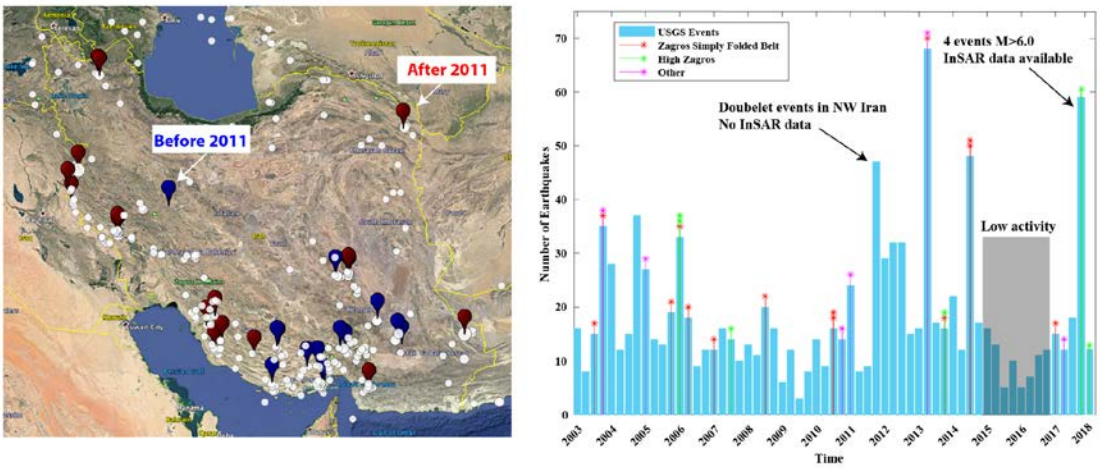

Figure 1. (left) Map of Iran with earthquakes. *Blue balloons, InSAR events between 2003 and 2011 as reported by Barnhart et al. [2013]; Red balloons, InSAR events after 2011; White circles, M>=5 earthquakes between 1/1/2003-2/1/2018 in the USGS catalog.* (right) Quarterly number of events with magnitude greater then 5. *Between 2003-2011, about 15 events were ground-truth with InSAR. Number of InSAR events is 2 in 2013, 3 in 2014, 0 in 2015 and 2016, 6 in 2017, and 1 in 2018. InSAR satellites are at minimum in year 2012 so missed at least two events. On average, it is about two events every year.*

Table 1. List of InSAR ground-truth events in Iran.

Event	Date	Lon° (+/-km)	Lat° (+/-km)	Depth (km)	Strike	Dip	Rake	Mw (GMT/ InSAR)	Reference
Zagros Simply Folded Belt				InSAR	InSAR	InSAR	InSAR		
1	05/05/97	53.881 (+/-0.3)	27.130 (+/-0.3)	5.2 (+/-0.3)	120*	80 (+/-4)	-90 (+/-6)	5.4	1
2	09/18/97	53.942 (+/-0.2)	27.083(+/-0.2)	3.5 (+/-0.2)	270*	85 (+/-6)	91 (+/-5)	5.3	1
3	10/01/98	54.245 (+/-0.3)	28.677 (+/-0.1)	1.4 (+/-0.2)	110*	45 (+/-5)	-61 (+/-11)	4.6	1
4	04/30/99	53.628 (+/-0.25)	27.870 (+/- 0.22)	4.1 (+/- 0.18)	110*	42 (+/-6)	-85 (+/-7)	5.3	1
5	07/10/03	54.175 (+/-2.5)	28.397(+/-1.5)	4.7 (+/-1.2)	274 (+/- 20)	36 (+/- 10)	97 (+/-12)	5.7/5.9	2
6	11/28/03	54.138 (+/- 0.49)	28.435 (+/- 0.37)	4.0 (+/- 0.38)	271 (+/- 4)	34 (+/- 6)	90 (+/- 17)	5.0/5.3	2
		54.151 (+/- 0.20)	28.429 (+/- 0.11)	3.8 (+/- 0.21)	94 (+/- 3)	48 (+/- 2)	105 (+/- 12)		
7	11/27/05	55.916 (+/-0.15)	26.809 (+/- 0.25)	6 (+/-0.3)	264 (+/-3)	47 (+/-4)	68 (+/-9)	5.9/6.1	2
		55.933 (+/-0.10)	26.813 (+/- 0.20)	5.8 (+/- 0.21)	74 (+/- 3)	35 (+/-3)	66 (+/-3)		
8	03/25/06	55.673 (+/- 0.86)	27.555 (+/- 0.83)	9.6 (+/- 0.71)	252 (+/-4)	34 (+/-4)	105 (+/-9)	5.9/6.0	2
		55.705 (+/- 0.74)	27.568 (+/- 0.78)	10.2 (+/- 0.51)	72 (+/- 3)	50 (+/-3)	95 (+/-3)		
9	06/28/06	55.966 (+/-0.43)	26.923 (+/- 0.57)	6.9 (+/- 0.35)	205 (+/-5)	31 (+/-5)	68 (+/-12)	5.8/6.1	2
		55.955 (+/-0.56)	26.916 (+/- 0.61)	9.1 (+/- 0.95)	45 (+/- 5)	64 (+/-3)	112 (+/-9)		
10	03/23/07	55.293 (+/-0.74)	27.603 (+/- 0.50)	4.0 (+/- 0.64)	285 (+/-7)	31(+/-10)	68 (+/-18)	5.0/5.3	2
11	09/10/08	55.924 (+/-0.31)	26.903 (+/- 0.47)	6.0 (+/- 0.38)	206 (+/-3)	14(+/-3)	81(+/-8)	6.1/6.3	2
		55.939 (+/- 0.32)	26.894 (+/- 0.52)	6.9 (+/- 0.41)	35 (+/- 2)	56 (+/-3)	99 (+/-10)		
12	07/20/10	53.842 (+/- 0.46)	27.118 (+/- 0.55)	4.3 (+/- 0.55)	237 (+/-7)	28 (+/-9)	57 (+/-14)	5.8/5.8	2
		53.860 (+/-0.16)	27.098 (+/- 0.33)	4.6 (+/- 0.29)	69 (+/- 1)	42 (+/-6)	73 (+/-2)		
13	04/09/13	51.746	28.493	7.6 (+/-0.3)	144 (+/-1)	48 (+/- 2)	95 (+/-4)	6.4	3
		51.867	28.302	3.6 (+/-0.4)	132 (+/-1)	40 (+/- 4)	107 (+/-10)		
14	08/18/14	47.695	32.703	6.5(+/-3.5)	Np1: 121/11 3/104 Np2: 308/31 7/320 (USGS	Np1: 79/65/63 Np2: 12/27/32 (USGS/CM T/ISC)	Np1: 89/80/72 Np2: 97/111/121 (USGS/CMT /ISC)	6.2	4

Table 1 (Continued). List of InSAR ground-truth events in Iran.

					/CMT/ISC)				
15	08/18/14	47.704	32.583					6.0**	4
16	12/30/14	51.900	28.720	1.5	302/195	75/41	54/157	5.4	5
17	01/06/17	53.18(+/-0.1)	28.15(+/-0.2)	1.8(+/-0.2)	156(+/-4)	24(+/-5)	97(+/-10)	5.0	6
High Zagros									
18	02/28/06	56.923 (+/- 1.1)	28.086 (+/- 1.1)	15.1 (+/- 1.2)	302 (+/- 21)	20 (+/- 5)	109 (+/- 19)	6.0/6.0	2
		56.983 (+/-1.3)	28.111 (+/-1.0)	14.8 (+/- 1.2)	93 (+/- 4)	71 (+/-4)	53 (+/-10)		
19	03/21/06	48.928 (+/- 0.62)	33.624 (+/- 0.54)	9.3 (+/- 1.2)	323(+/- 2)	68 (+/- 5)	111(+/- 9)	6.1/6.2	2
20	08/25/07	56.723 (+/-0.19)	28.247 (+/- 0.21)	2.8 (+/- 1.0)	230(+/- 2)	80 (+/- 7)	19 (+/- 10)	5.0/5.0	2
21	05/11/13	57.770	26.560	6.0	259	89	-3	6.1	7,8
22	11/22/13	45.63(+/-0.5)	34.36(+/-0.6)	8(+/-1.0)	335(+/- 6)	35(+/-4)	90(+/-10)	5.8	6
23	11/12/17	45.959	34.911					7.3	6
24	12/01/17	57.314	30.743					6.1	6
25	12/12/17	57.280	30.737					6.0	6
26	12/12/17	57.298	30.828					6.0	6
27	01/11/18	45.678	33.790					5.5	6
Other									
28	12/26/03	58.362 (+/- 0.38)	29.018 (+/- 0.98)	7.6 (+/-3.4)	175 (+/-2)	82 (+/- 3)	178 (+/-10)	6.6/6.6	2
29	02/22/05	56.842 (+/- 4.2)	30.795 (+/- 4.1)	2.5 (+/- 1.8)	79 (+/- 7)	64 (+/- 8)	101(+/- 23)	6.4/6.4	2
30	12/20/10	59.121 (+/- 2.1)	28.244 (+/- 2.4)	5.3 (+/- 2.8)	30 (+/- 2)	89 (+/-8)	178 (+/-2)	6.5/6.5	2
31	01/27/11	59.047 (+/-0.41)	28.163 (+/- 0.41)	10.0 (+/- 2.8)	123 (+/- 3)	90 (+/-2)	2 (+/-5)	6.2/6.3	2
32	04/05/17	60.39(+/-0.4)	35.76(+/-0.6)	4.8(+/-2.0)	319(+/- 5)	50(+/-7)	135(+/-10)	6.1	6

- * indicate values that were fixed during inversion. The error bounds on the rest of the mechanism would be larger by ~10 degree if they did not fix these parameters, but the error bounds on depth would be only slightly altered.
- ** This event is a doublet events with two earthquakes with similar size. The Motagh et al., 2015 did not separate the solution nor provide the uncertainty estimation.
- Black: events before 2011 reported by other researchers
- Green: events after 2011 reported by other researchers
- Red: Found and analyzed by this project
- Blue: Found but not analyzed by this project
- Reference: 1: Lohman and Simons, 2005; 2: Barnhart et al. 2013; 3: Elliott et al., 2015; 4: Motagh et al, 2015; 5: Ammon, TIM talk 2017; 6: This report; 7: Samsonov and Czarnogorska, 2013; 8: Penney et al., 2015

We applied our grid search method to three selected events. Here we report two events in detail: the April 5, 2017 M6.1 Sefid Sang earthquake (event 32 in table 1) and the January 6, 2017 M5.0 Chah Tala event (event 17 in table 1). The Chah Tala event is

small but the signal is clear, allowing us to get a good comparison with seismic inversion. The Sefid Sang earthquake is much larger with signal span over 20 km. The uncertainty of parameters was determined based on how misfit changes with the parameters. We also tested a new method to remove atmosphere noise based on topography to the InSAR data of the Sefid Sang earthquake.

M6.1 Sefid Sang event

On April 5, 2017, an M6.1 earthquake struck near the village of Sefid Sang, Iran, with two recorded fatalities.

The tectonics of the region is driven by the convergence of the Arabian and Eurasian plates. While most of the shortening is accommodated over southern and central Iran, the region around the Sefid Sang event is still experiencing a convergence rate of several millimeters per year [Masson et al., 2007]. Several strike-slip faults run across the region, allowing rigid blocks to move aside to accommodate the shortening [Shabanian et al., 2009].

The location of the Sefid Sang event does not appear directly on any known faults, but it lies southeast of the end of the Kashafrud Fault [Sheikholeslamia and Kouhpeyma, 2012]. Berberian [1981] mapped the Kashafrud Fault as a northward-dipping reverse fault with a component of right-lateral strike slip. Although there are no large events on the Kashafrud Fault, there are historical records of two events on the fault in the seventeenth century [Berberian, 1979], one strike slip event and one reverse event [Berberian, 1981].

Our inversion shows an oblique slip event with unique source properties. Dipping towards the south with a dip of 50˚, it is more steeply dipping than a typical thrust event, and with a rake of 135˚, its source mechanism is halfway between thrust and left-lateral strike slip.

The focal mechanism of the Sefid Sang event appears almost opposite to the motion of the Kashafrud Fault, making it unlikely that the event represents a continuation of the Kashafrud Fault. Instead, we hypothesize that the left-lateral component of the Sefid Sang event may originate from release of strain accumulated along the Kashafrud Fault since its two seventeenth century earthquakes.

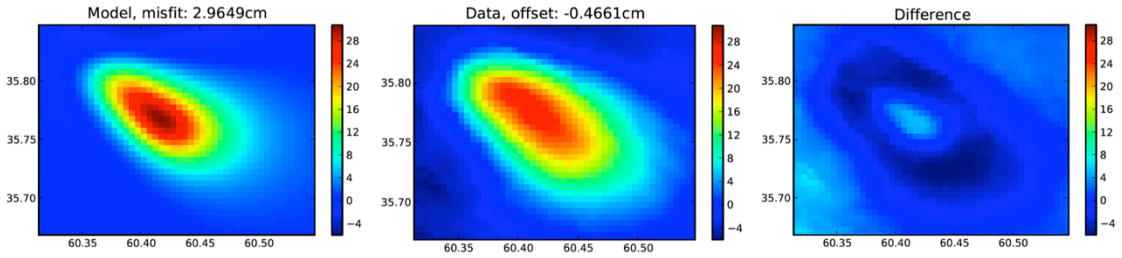

Figure 2. InSAR observation and modeling of the April 5, 2017 M6.1 Sefid Sang earthquake.

M5.0 Chah Tala event

On January 6, 2017, an M5.0 earthquake struck near the village of Chah Tala, Iran. The shallow event occurred beneath flat farmland, minimizing the distortions and allowing a highly accurate detection by InSAR. Because of the small size, it allowed an unprecedented accuracy in the determination of its location.

While the Harvard GCMT solution had indicated a large component of oblique slip, our geodetic inversion suggests a rake of 93˚, indicating an event very close to pure thrust (90˚). The interferogram shows a clear negative field, so it contains more data about the source parameters than it would with just a positive field.

The strike (153˚) and dip (24˚) are consistent with many deeper thrust events that accommodate the shortening across the Zagros Mountains, but the depth of 1.84 km is unusually shallow.

The event lies below the center of a flat, 7 km-wide valley stretching between two ridges composed of dipping Eocene layers. The valley fill consists of Miocene and Quaternary sediments, and the depth of the event is consistent with the Miocene sediments, the Miocene-Eocene unconformity, or a fault connecting the two Eocene units beneath the valley fill.

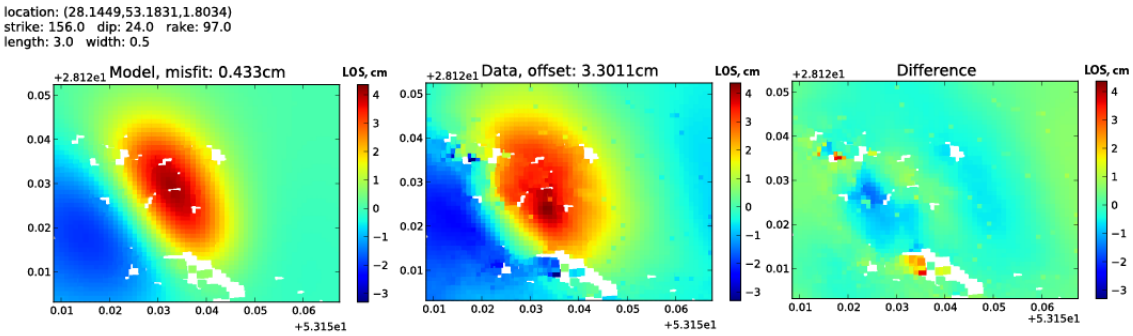

Figure 3. InSAR observation and modeling of the January 6, 2017 M5.0 Chat Tala earthquake.

Shear modulus

Because the shear modulus structure of the Earth is not uniform, the assumption of a uniform half space is a problematic one. In the Zagros mountains of Iran, where most of our events take place, the subsurface strata contain multiple dipping sedimentary layers over a crystalline basement with a substantially different shear modulus [Barnhart and Lohman, 2013]. Unfortunately, however, it is not always possible to obtain complete data about the subsurface structure, and a more complex model, while mathematically possible, would be substantially more computationally expensive.

We choose our uniform shear modulus to be 30 GPa. This assumption will produce meaningful errors in depth, but it is unavoidable without detailed knowledge of the source rock properties. To test the effect, we compared synthetic InSAR signals from two events. In figure 4, model 1 and 2 has the same fault geometry. However, model 2 has 0.5 effective normal stress and twice the slip, keeping the seismic moment the same. Model 2 produced much larger surface deformation. This suggested that to match the same InSAR observation, the depth of the best fitting model for a smaller shear modulus should be larger than the reference shear modulus. To quantify the difference, one may treat shear modulus as a parameter to search for the best fitting model. However, this will introduce another parameter and increase the computational burden using our grid search approach, so we did not explore further in this project. In the future, we suggest use statistic method such as the Bayesian approach to quantify the uncertainty. It is much more efficient than the grid search approach and the additional parameter of shear modulus can be handled.

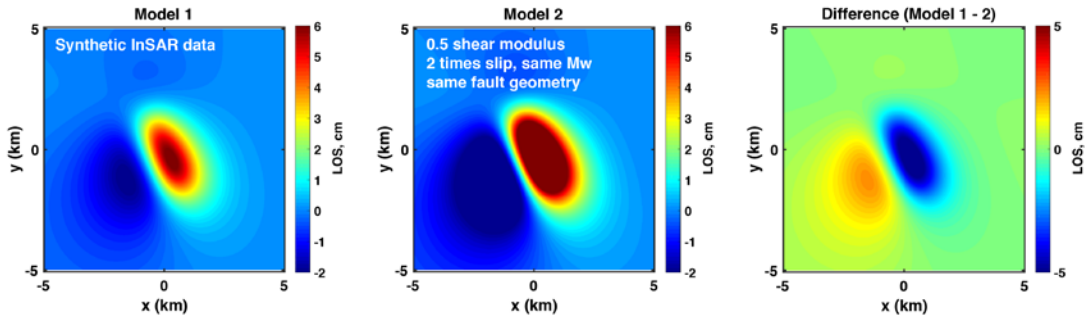

Figure 4. The effect of reduced shear modulus for a thrust event. *Model 1: dip 24°, strike 156°, rake 90°, length 3.0, width 0.5 km, slip 1.0 m, depth 1.5 km (top of the fault model), and 30 GPa shear modulus. Model 2: 1/2 of shear modulus as Model 1 but twice slip, to keep the moment magnitude the same. The difference is quite large. The best-fitting slip model using reduced shear modulus should be deeper than model 1.*

Using topography to reduce atmospheric noise

We applied the topographic correction of InSAR data to the Sefid Sang earthquake (Figure 5). The standard deviation of the original unwrapped interferogram is 17.35, whereas the corrected interferogram standard deviation is significantly less at 2.82. There is also a decrease in means, with the original interferogram having a mean of 0.97 mm and the corrected one with a mean of -0.20. This demonstrated that the topography-correction worked well for this case.

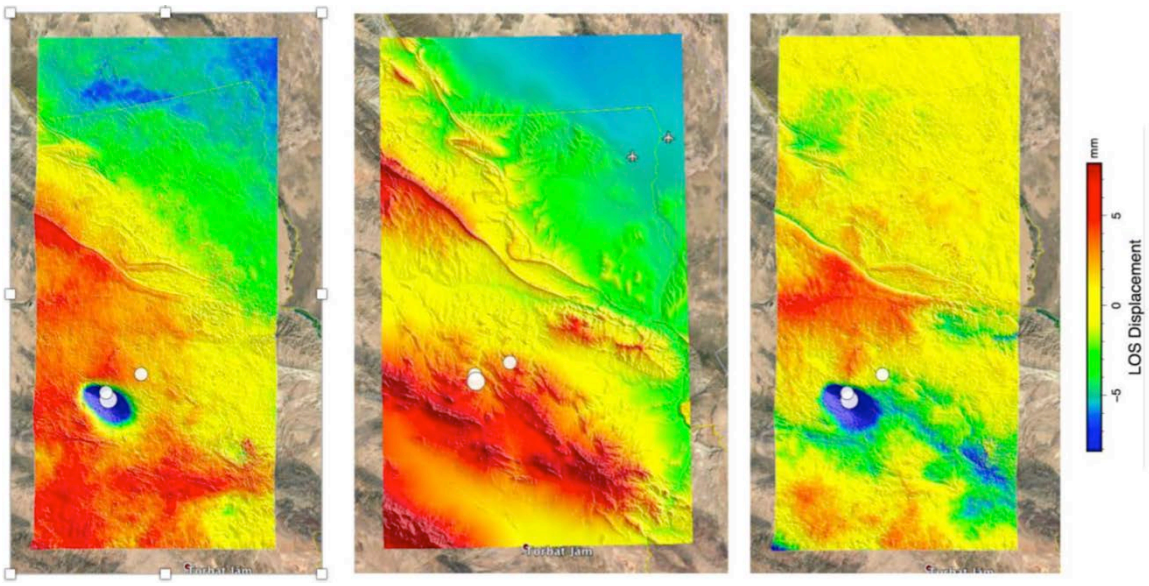

Figure 5. Effect of topographic noise reduction on InSAR observations. (left) Original interferogram. *The white circles are the M6.1 Sefid Sang earthquake and its two aftershocks.* (middle) Predicted phase change based on topography. (right) The difference between original and the topo-predicted phase.

4.2. Seismic inversion

We applied full waveform seismic inversion to several events. Here we highlighted the result for the Chat Tala event. We used data of about 10 GNS seismic stations, which were downloaded from IRIS DMC. We fit data for all three components. Figure 6 shows the different focal mechanisms with different assumption of location and depth. We varied the location by about every 5 km in both latitude and longitude near the InSAR identified location (blue beach ball in Figure 6). We also varied the depth every kilometer. The focal mechanism does not change much with location but is sensitive to depth. InSAR inversion suggested that the depth is quite shallow, in the top 2 km. In contrast, GCMT reported this event at 12 km depth, and their focal mechanism is shown as a red beach ball in Figure 6. Their solution is close to our seismic inversion at that depth but quite different from our preferred solution based on InSAR determined depth.

Barnhart et al. [2013] proposed that some InSAR observed signal was triggered aseismic slip at shallow depth. The Chat Tala event is probably not the case because the shallow signal can be well explained by a M5.0 fault slip and it is hard to imagine that an earthquake at this size at much deeper depth (12 km) could trigger so much shallow aseismic slip. The Chat Tala event really shows the advantage of having both InSAR signal and seismic data.

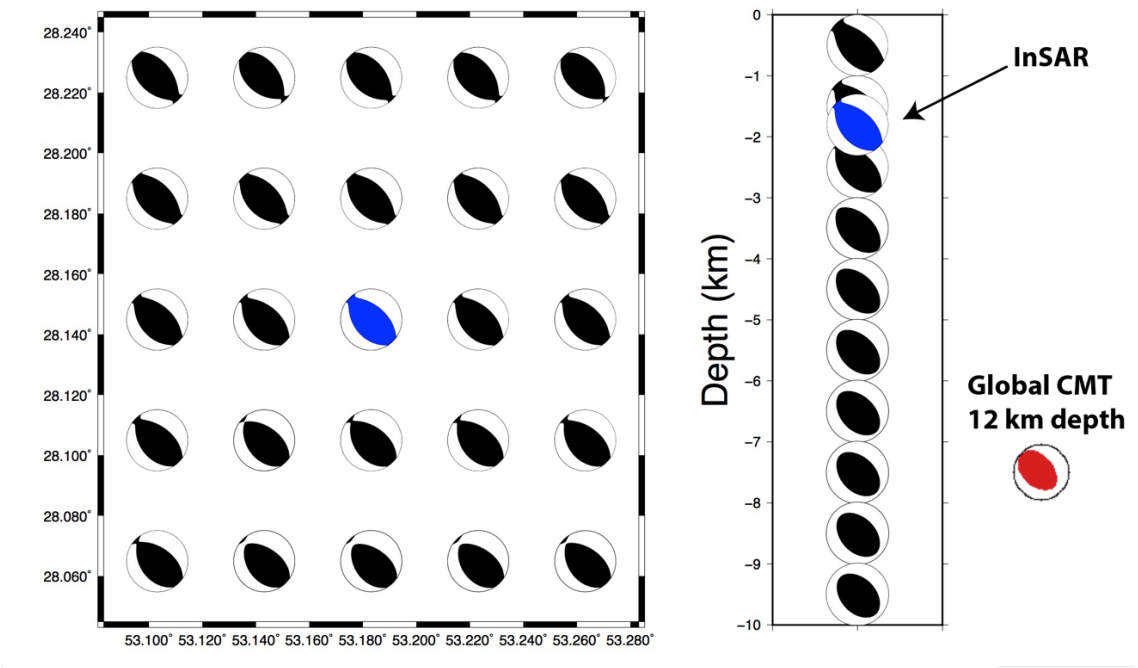

Figure 6. Focal mechanism solution for seismic inversion of the Chat Tala M5.0 earthquake.

4.3. Relative relocation with surface waves

We started the relocation by using M≥4.5 earthquakes in Iran in the USGS catalog. The search area is latitude 24.49-40.28N and longitude 43.39-64.11E and the search time window is between January 1970 – October 2017. Figure 7 shows the distribution of these 3304 earthquakes and the 88257 selected pairs of earthquakes, which have been identified based on the following criteria: within 120 km distance, 10 km depth, and 1 magnitude from the references. Of these earthquake pairs, 500 (~0.6%) have an average correlation over 0.6 with more than 10 seismic stations. The low percentage of good pairs is mainly due to two reasons. First, the number of GNS stations remained small until early 1990s. There were fewer stations available for any pair with earthquakes earlier than 1990s. Second, many pairs have different focal mechanisms that making the correlation of Rayleigh surface wave low. However, because of the relative large number of pairs, we still relocated 86 of M≥4.5 earthquakes using InSAR events as reference. The number of relocated earthquakes will likely be increased over time and also when we look for earthquakes with lower magnitude such as (M<4.5).

We calculated the distance between these 86 pairs in the USGS catalog and with updated locations. The histogram of the differences is shown in figure 8. For the distance, about 6% are within 5 km and 26% within 10 km (Figure 8a). The rest 74% are beyond 10 km and about 36% are beyond 50 km. For the uncertainty, 80% are within 5 km (Figure 8b). This shows that the relocations have significantly improved the relative locations, and likely relocated many events are previously incorrectly located. The location difference

between the USGS catalog and our relocated events peaks at about 16 km with an average of 54 km (Figure 9).

The location uncertainty of a relocated event can be less than 5 km, even if the reference event is large (Figure 9). The rupture length of a large (M>6) reference event can be over 20 km and the epicenter can be anywhere on the fault. Therefore, the uncertainty of epicenter of a large reference event can be as large as 10-20 km. However, InSAR data can constrain the centroid really well, usually within a few hundreds of meters. The relative relocation using surface wave method will constrain the distance between the centroid of earthquakes, instead of epicenter. So, the uncertainty of the centroid location of a relocated event is the sum of the uncertainty of reference centroid (~100s of meters) and the uncertainty of the relative distance between the reference and relocated event (< 5 km). As long as the relocated event is small, the difference between its centroid and epicenter is small. So, the final uncertainty of the epicenter of a relocated event can be as small as 5 km.

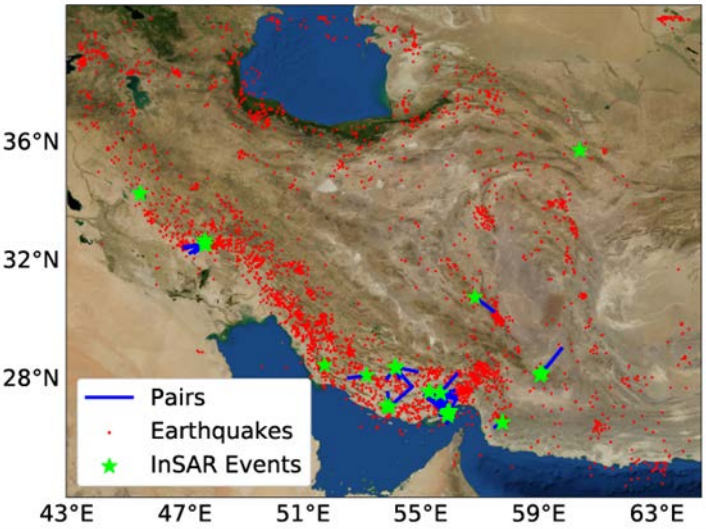

Figure 7. Earthquakes M > 4.5 in Iran used in the relocation (Latitude 20.49-40.28N; Longitude 43.39-64.11E). *Data are from the USGS catalog between January 1970 – October 2017. The blue lines link the 86 good pairs of relocated events with their references.*

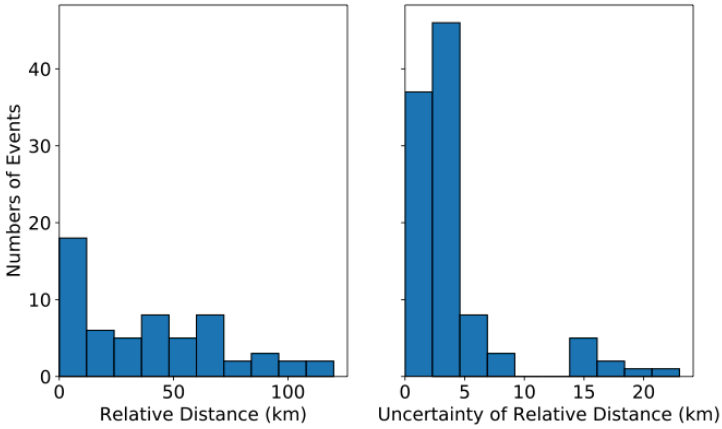

Figure 8. (a) Histogram of distance between relocated events and the reference events. (b) Histogram of uncertainty of relative location between relocated events and the reference events.

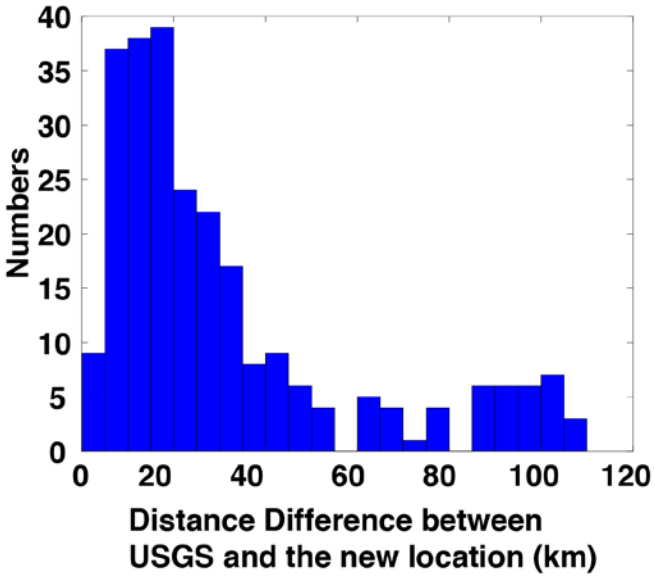

Figure 9: Histogram of the distance difference of relocated pairs between the USGS catalog and the new location.

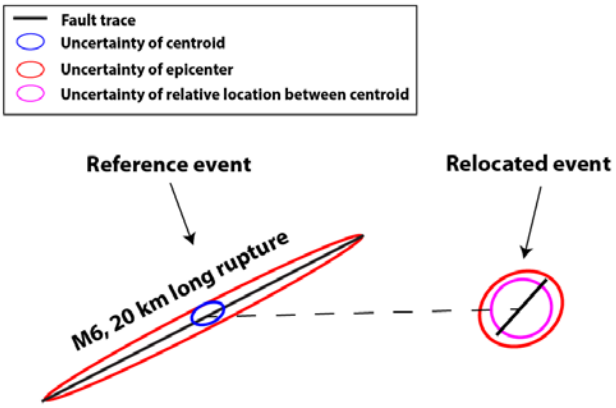

Figure 10. Diagram to show that the location uncertainty of relocated events can be as small as 5 km even the reference event has a 20 km fault rupture. *The key is that surface wave cross-correlation determines the relative distance between centroid instead of epicenter. The large uncertainty of epicenter of the reference event is irrelevant.*

5. CONCLUSIONS

InSAR is an effective and independent method to ground truth earthquakes. We extended previous research beyond 2011. Together, this added the total number of InSAR events in Iran to 32. We developed a grid search approach on geodetic inversion, which can be combined with seismic inversion to provide improved constraints on source parameters including focal mechanism, location and depth. This method is most effective for small events (M<6). The impact of ground truth events was amplified when coupled with relative relocation method such as the surface wave cross-correlation method. Using surface wave, we were able to relocate more than 80 M≥4.5 earthquakes in the USGS catalog. The number of these relocated events will increase as time goes on because the

method can be applied to relocate earlier events as long as enough stations were in operation.

6. RECOMMENDATIONS

(1) The list of InSAR ground-truthed events might not be complete. For example, the 2014 M5.4 Boshkan on the list was not noticed by our team until Charles Ammon reported it at the 2017 AFRL TIM meeting. The reason was that USGS assigned 28 km depth for this event and we did not include it in our InSAR data analysis due to the limited labor and time. The final depth turned out to be quite shallow based on InSAR inversion at Penn State (~1.5 km). Some automatic scanning algorithm would be required to fully taking advantage of the abundance of InSAR data and earthquakes in Iran.
(2) The relocated events by this project have not been reported to any catalog or agency. More detailed work is needed to validate these relocations. Once it is done, we should be able share our results with the community.
(3) We used misfit between data and forward model to estimate the uncertainty of our fault parameters. A better approach would be to use some Bayesian-based inversion method because the uncertainty has statistical meaning. We recommend applying a Bayesian-based approach to all the previous and future InSAR reference events.

Note:
Sam Bell also explored two ideas to improve the earthquake location estimate. However, neither ended up publishable results before he left for a new job. Here we summarize them below:

(1) Bayesian inversion of geodetic data. As mentioned earlier, the grid search method for geodetic modeling took a long time to run. We need to reduce the number of parameters to make the calculation manageable and find a better way to estimate the uncertainty. A promising method would be to use Bayesian based inversion method. Sam Bell wrote a Bayesian inversion code in Python but the results were not as expected. He did not have time to further improve the code.
(2) Relocate earthquakes with different mechanism. A limitation of the surface wave cross-correlation method is that only earthquakes with similar focal mechanism can be correlated well. Sam attempted to get around it by using full-waveform forward modeling of two events using GCMT solution. Then the modeled waveform will be compared with recorded waveforms in a double-difference manner. However, a large number of events need to be calculated to take advantage of the double-difference method, which makes it computationally too costly. Sam stopped the effort after a few tries.

REFERENCES

Barnhart, W. D. and R. B. Lohman (2013), Vertical partitioning of strain during earthquake sequences in Iran: Phantom earthquakes and triggered aseismic creep, Geophys. Res. Lett., 40, pp. 819-823, doi:10.1002/grl.50201.

Barnhart, W. D., R. B. Lohman, and R. J. Mellors (2013), Active accommodation of plate convergence in Southern Iran: Earthquake locations, triggered aseismic slip, and regional strain rates, J. Geophys. Res. Solid Earth, 118, pp. 5699-5711, doi:10.1002/jgrb.50380.

Bekaert, D., R. Walters, T. Wright, A. Hooper, and D. Parker (2015), Statistical comparison of InSAR tropospheric correction techniques. Remote Sensing of Environment, 170, pp. 40-47, doi:10.1016/j.rse.2015.08.035.

Berberian, M. (1979), Evaluation of the instrumental and relocated epicentres of Iranian earthquakes, Geophysical Journal International, DOI: 10.1111/j.1365-246X.1979.tb04798.x.

Berberian, M. (1981), Active Faulting and Tectonics of Iran, in Zagros Hindu Kush Himalaya Geodynamic Evolution (eds H. K. Gupta and F. M. Delany), American Geophysical Union, Washington, DC, doi: 10.1029/GD003p0033.

Bondar, I. and K. L. McLaughlin (2009), A New Ground Truth Data Set For Seismic Studies. Seismological Research Letters, 80(3), pp. 465-472, http://doi.org/10.1785/gssrl.80.3.465.

Cleveland, K. M. and C. J. Ammon (2013), Precise relative earthquake location using surface waves, J. Geophys. Res. Solid Earth, 118, pp. 2893-2904, doi: 10.1002/jgrb.50146.

Ekström, G., M. Nettles, and A.M. Dziewonski (2012), The global CMT project 2004-2010: Centroid-moment tensors for 13,017 earthquakes, Phys. Earth Planet. Int., pp. 200-201, 1-9.

Elliott, J. R., E. A. Bergman, A. C. Copley, A. R. Ghods, E. K. Nissen, B. Oveisi, and F. Yamini-Fard (2015), The 2013 Mw 6.2 Khaki-Shonbe (Iran) Earthquake: insights into seismic and aseismic shortening of the Zagros sedimentary cover, Earth and Space Science, http://doi.org/10.1002/2015EA000098.

Engdahl, E. R. and E. A. Bergman (2001), Validation and generation of reference events by cluster analysis, 23rd Seismic Research Review, Jackson Hole, WY.

Hauksson, E. and P. Shearer (2005), Southern California hypocenter relocation with waveform cross-correlation, Part 1: Results using the Double-Difference method, Bull Seismol. Soc. Am., 95, pp. 896-903, doi: 10.1785/0120040167.

Kikuchi, M. and H. Kanamori (1991), Inversion of complex body waves – III, Bull. Seismol. Soc. Am., 81, pp. 2335-2350.

Liu, Q., J. Polet, and D. Komatitsch (2004), Spectral-Element Moment Tensor Inversions for Earthquakes in Southern California, Bulletin of the Seismological Society of America, 94(5), pp. 1748-1761, http://doi.org/10.1785/012004038.

Lohman, R. B. and M. Simons (2005), Locations of Selected Small Earthquakes in the Zagros Mountains, G-cubed 6, Q03001, doi:10.1029/2004GC000849.

Masson, F., M. Anvari, Y. Djamour, A. Walpersdorf, F. Tavakoli, M. Daignières, and S. Van Gorp (2007), Large-scale velocity field and strain tensor in Iran inferred from GPS measurements: New insight for the present-day deformation pattern within NE Iran, Geophysical Journal International, 170(1), pp. 436-440. http://doi.org/10.1111/j.1365-246X.2007.03477.x.

McGuire, J. J. (2008), Seismic Cycles and Earthquake Predictability on East Pacific Rise Transform Faults, Bulletin of the Seismological Society of America, 98(3), pp. 1067-1084, doi:10.1785/0120070154.

Motagh, M., A. Bahroudi, M. H. Haghighi, S. Samsonov, E. Fielding, and H.-U. Wetzel (2015), The 18 August 2014 Mw 6.2 Mormori, Iran, Earthquake: A Thin-Skinned Faulting in the Zagros Mountain Inferred from InSAR Measurements, Seismological Research Letters, 86(3), pp. 775-782. http://doi.org/10.1785/0220140222.

Okada, Y. (1985), Surface deformation due to shear and tensile faults in a half-space, Bull. Seismol. Soc. Am., 75, pp. 1135-1154.

Penney, C., A. Copley, and B. Oveisi (2015), Subduction tractions and vertical axis rotations in the Zagros-Makran transition zone, SE Iran: The 2013 May 11 Mw6.1 Minab earthquake, Geophysical Journal International, 202(2), pp. 1122-1136. http://doi.org/10.1093/gji/ggv202.

Poupinet, G., W.L. Ellsworth, and J. Frechet (1984), Monitoring velocity variations in the crust using earthquake doublets: An application to the Calaveras Fault, California, J. Geophys. Res., 89, pp. 5719-5731.

Samsonov, S.V. and M., Czarnogorska (2013), Ground deformation produced by 2013 M6.1 Minab earthquake in Iran mapped with RADARSAT-2 DInSAR, Geological Survey of Canada, Open File 7528, doi:10.4095/293320.

Schaff, D.P. and F. Waldhauser (2005), Waveform cross-correlation-based differential travel-time measurements at the Northern California seismic network, Bull. Seismol. Soc. Am., 95, pp. 2446-2461, doi: 10.1785/0120040221.

Shabanian, E., L. Siame, O. Bellier, L. Benedetti, and M. R. Abbassi (2009), Quaternary slip rates along the northeastern boundary of the Arabia-Eurasia collision zone (Kopeh Dagh Mountains, Northeast Iran), Geophysical Journal International, 178(2), pp. 1055-1077, http://doi.org/10.1111/j.1365-246X.2009.04183.x.

Shearer, P.M. (1997), Improving local earthquake locations using the L1 norm and waveform cross correlation: Application to the Whittier Narrows, California, aftershock sequence, J. Geophys. Res., 102, pp. 8269-8283.

Sheikholeslami, M. R. and M. Kouhpeyma (2012), Structural analysis and tectonic evolution of the eastern Binalud Mountains, NE Iran, Journal of Geodynamics, 61, pp. 23-46, http://doi.org/10.1016/j.jog.2012.06.010.

Vincent, P., S. Larsen, D. Galloway, R. J. Laczniak, W. R. Walter, W. Foxall, and J. J. Zucca (2003), New signatures of underground nuclear tests revealed by satellite radar interferometry, Geophys. Res. Lett., 30, p. 2141, doi:10.1029/2003GL018179, 22.

Waldhauser, F. and W.L. Ellsworth (2000), A double-difference earthquake location algorithm: Method and application to the northern Hayward fault, California, Bull. Seism. Soc. Am., 90, pp. 1353-1368.

Zhao, L., P. Chen, and T. H. Jordan (2006), Strain Green tensor, reciprocity, and their applications to seismic source and structure studies, Bull. Seism. Soc. Am., 96, pp. 1753-1763, doi:10.1785/0120050253.

Zhu, L. and D. V. Helmberger (1996), Advancement in source estimation techniques using broadband regional seismograms, Bulletin of the Seismological Society of America, 86(5), pp. 1634-1641.

List of Symbols, Abbreviations, and Acronyms

AFRL	Air Force Research Laboratory
CMT	Centroid Moment Tensor
DMC	Data Management Center
GCMT	Global Centroid Moment Tensor
GT	Ground-truth
HPC	High Performance Computer
InSAR	Interferometric Synthetic Aperture Radar
IRIS	Incorporated Research Institutions for Seismology
SGT	Strain Green Tensor
TIM	Technical Interchange Meeting
USGS	United States Geological Survey

DISTRIBUTION LIST

DTIC/OCP
8725 John J. Kingman Rd, Suite 0944
Ft Belvoir, VA 22060-6218 1 cy

AFRL/RVIL
Kirtland AFB, NM 87117-5776 1 cy

Official Record Copy
AFRL/RVBYE/Dr. Frederick Schult 1 cy